

Collaborative Target Search with a Visual Drone Swarm: An Adaptive Curriculum Embedded Multi-stage Reinforcement Learning Approach

Jiaping Xiao, Phumrapee Pisutsin and Mir Feroskhan, *Member, IEEE*

Abstract—Equipping drones with target search capabilities is desirable for applications in disaster management scenarios and smart warehouse delivery systems. Instead of deploying a single drone, an intelligent drone swarm that can collaborate with one another in maneuvering among obstacles will be more effective in accomplishing the target search in a shorter amount of time. In this work, we propose a data-efficient reinforcement learning-based approach, Adaptive Curriculum Embedded Multi-Stage Learning (ACEMSL), to address the challenges of carrying out a collaborative target search with a visual drone swarm, namely the 3D sparse reward space exploration and the collaborative behavior requirement. Specifically, we develop an adaptive embedded curriculum, where the task difficulty level can be adaptively adjusted according to the success rate achieved in training. Meanwhile, with multi-stage learning, ACEMSL allows data-efficient training and individual-team reward allocation for the collaborative drone swarm. The effectiveness and generalization capability of our approach are validated using simulations and actual flight tests. The code is available at <https://github.com/NTU-UAVG/collaborative-target-search-vision-drone-swarm.git> and the video is at <https://youtu.be/LuCK97i5Bcw>.

Index Terms—Multi-agent systems, collaborative target search, deep reinforcement learning, curriculum learning, drones.

I. INTRODUCTION

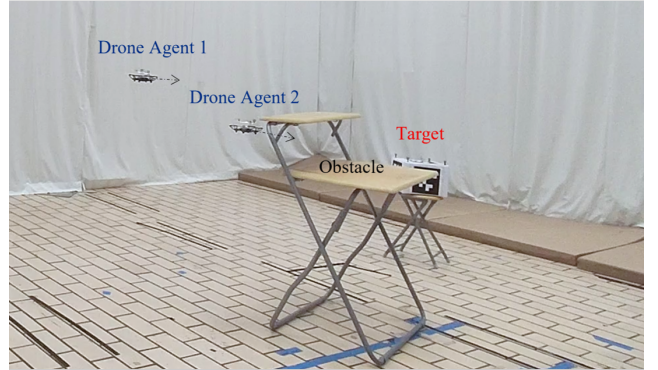
As microelectronic technology, sensors, and onboard computing capabilities have achieved tremendous advancement in recent years, autonomous micro-drones have been widely used in various target search missions [1], [2]. Target search with autonomous agents is increasingly required in smart warehouse delivery systems [3] and disaster management scenarios [4] such as parcel pickup & delivery and building collapse rescue. Such scenarios require time-efficient environment exploration, object detection and recognition, and navigation in cluttered environments. Nevertheless, because of the limited sensing range of a single drone, a drone swarm is favored for a large scale environment exploration task due to more available observation information and parallel task execution capabilities. A drone swarm with the formation maneuvering capability has been massively studied for fulfilling such large scale tasks, which require information on relative positions [5], [6] or bearings [7] to achieve a desired geometric shape without significant collaborative behaviors.

Manuscript received February 27, 2022. This work was supported by the Ministry of Education, Singapore, under its Academic Research Fund Tier 1 (RG69/20).

J. Xiao, P. Pisutsin and M. Feroskhan are with the School of Mechanical and Aerospace Engineering, Nanyang Technological University, Singapore 639798, Singapore (e-mail: jiaping001@e.ntu.edu.sg; pisu0001@e.ntu.edu.sg; mir.feroskhan@ntu.edu.sg).



(a)



(b)

Fig. 1. (a) A honeybee swarm is searching for nectar collaboratively [<https://www.gettyimages.com/photos/bee>]. (b) A visual drone swarm is searching for a target parcel box controlled by reinforcement learning.

However, collaborative behavior among agents such as maneuvering in cluttered environments [8], [9] without collision with obstacles and other agents while target searching are essential for a drone swarm to carry out the aforementioned tasks. Collaborative Target Search (CTS) behavior is usually observed among intelligent biological swarms [10] such as honeybees searching for nectar (see Fig. 1), ants finding food and birds looking for a living space. Attributing collaborative behavior to a drone swarm is challenging, as drone agents must acquire intelligent decision-making capabilities in the absence of swarm leaders and knowledge of the map of the environment.

Recently, deep reinforcement learning (DRL) [11] has been widely applied in robots for environment exploration [12], [13]

and target-driven visual navigation [14]–[16] in unknown environments. However, differentiating from the full environment exploration problem, our CTS problem aims to infer potential locations of a target instead of maximizing the area covered. Even though full environment exploration guarantees a feasible solution for target search, it would be more efficient for agents to directly estimate with high probability the potential space containing the target. While the target-driven visual navigation with deep reinforcement learning utilizes purely visual perception and policy neural network to guide a robot through an indoor environment where the target is fixed within a spatial layout, our work focuses on multi-agent collaborative target finding and approaching over a 3D sparse reward space with limited visual perception and egocentric states where the target is randomly placed without prior knowledge. The success rate and the time to reach are the main metrics to evaluate the performance of CTS for a drone swarm.

In this paper, a visual drone swarm is adopted for CTS in an indoor environment to search for and approach a parcel box. A data-efficient deep reinforcement learning-based method is applied to find an optimal search policy with less time cost. There are several challenges to accomplishing this CTS task for drones. Firstly, the drone agents need to be driven to efficiently explore the 3D environment with sparse rewards. Secondly, the drone swarm is required to differentiate the target, obstacles and other collaborative agents with a forward color camera during flight. Lastly, the drone swarm should display collaborative behaviors for target search, i.e., without colliding into the obstacles or other agents.

To this end, we propose an Adaptive Curriculum Embedded Multi-Stage Learning (ACEMSL) approach to address these challenges. Compared to the standard curriculum learning methods [17], [18] where the learning curriculum involves pre-designed parameters that change across the training process, our approach divides the training process into two adaptive curriculum embedded stages. This can reduce the data required to achieve the best performance due to the self-adjustment capability of the curriculum. Meanwhile, CM3 in [19] has validated the data-efficiency and outstanding performance of multi-stage learning for cooperative multi-goal multi-agent tasks, such as cooperative navigation. Similar to CM3, in our approach, the single greedy agent is trained prior to multiple agents, collaborative learning. However, CM3 considers its two stages as a complete curriculum and requires knowledge of goal assignment, while the proposed ACEMSL embeds an adaptive curriculum into each stage without knowing the target’s location. In each stage, the probability of hiding the target from a drone swarm increases when the desired success rate is achieved. In this way, the drone agents are gradually guided to explore the environment with sparse rewards and try to search the potential locations of the target. To improve the efficiency of learning, the shared neural network among each agent is trained in a small size space and then transferred to an unseen larger sized environment. Domain randomization, which includes the initial state of drones, parameters of the target and the intensity of light, is adopted during the training process. In this paper, our main **contributions** are summarized as follows.

1) We propose an adaptive embedded curriculum (AEC) algorithm enabling drones to explore and navigate 3D cluttered environments with sparse rewards efficiently;

2) Without any prior knowledge of the target and the environment layout, we develop multi-stage reinforcement learning to train a scalable, decentralized drone swarm to find the target with only a color camera as visual perception;

3) To the best of our knowledge, our work is unprecedented in successfully transferring the trained policy model from simulation to a real-life visual drone swarm and demonstrate their CTS performance physically.

II. RELATED WORKS

A. Collaborative Target Search (CTS)

CTS tries to locate and reach the target using multi-agents while handling the environment exploration efficiently. The conventional idea to accomplish the CTS task is to formulate an optimization problem and break it down into local optimization sub-problems. There are two conventional ways to solve this local optimization problem, namely numerical analysis methods [8], [20] and heuristic methods [9], [21]–[23]. Under the category of numerical analysis methods, A. Dominik Haumann et al. [20] achieved the multi-robot exploration and path planning via optimization partition of the objective function for each agents. Dario Floreano et al. [8] adopted Nonlinear Model Predictive control (NMPC) to optimize the navigation performance of an aerial robotic swarm towards a targeted area in an indoor cluttered environment. The numerical analysis method necessitates the knowledge of precise agents’ dynamics and the complex computation for obtaining feasible solutions that satisfy constraints and boundary conditions. Hence, it will be challenging to extend the method to a large-scale swarm.

Under the category of heuristic methods, based on the genetic algorithm, Samira Hayat et al. [22] formulated a multi-objective optimization algorithm to allocate tasks and find a target in a bounded area for a team of UAVs. In [23], evolutionary algorithms (EAs) were developed to tackle criminals search problems with human-UAV collaboration. A search strategy based on the particle swarm optimization (PSO) was proposed in [9] for a nano drone swarm to localize a gas source in unknown and cluttered environments. The heuristic methods, on the other hand, can save modeling and computation resources but do not provide the guarantee of obtaining the global optimal solution for the drone swarm, resulting in sub-optimal or local search behaviors, which may lead to the failure of task.

B. Deep Reinforcement Learning

Collaborative exploration and target search in large-scale and cluttered environments may now be addressed more readily due to the feasibility and transfer capabilities of deep reinforcement learning. In the domain of drones [18], [24]–[26] and Multi-Agent Reinforcement Learning (MARL) problems [19], [27]–[30], deep reinforcement learning has achieved promising success. Current methods with DRL in drone scenarios are mostly applied to single drone tasks [18], [25], [26] or scenarios with discrete action spaces and grid

observation environments [19], [30]. In [18], an augmented curriculum learning was proposed to guide the drone to fly through a narrow gap. However, their curriculum can only vary along pre-designed rules which limiting reinforcement learning performance. With a global grid map, [24] proposed a Snake algorithm with DRL aiming to search a target using an autonomous UAV but failed to extend it to practical scenarios where only local visual observations are available. In [19], CM3 (Cooperative Multi-goal, Multi-stage, Multi-agent) was proposed for multi-agent reinforcement learning in 2D space to solve a collaborative navigation problem, where the positions of landmarks and goals were known to each agent. Besides, function augmentation was adopted in CM3 to bridge the agent's own state in stage 1 and the egocentric observations in stage 2. However, this the scalability of the trained model since a new model needs to be trained if the number of agents changed. [29] proposed a two-level reinforcement learning-based control method for a UAV swarm to perform surveillance in an unknown 3D urban area collaboratively. However, the approach requires each UAV to have information on the target's position and requires the environment to be constructed in grids with regular shaped blocks to enable the agents to differentiate the obstacles and the target easily. This limits the application of this method in real-life scenarios.

However, exploring a 3D unstructured environment and searching a hidden target with a visual drone swarm is more challenging since the 3D reward space is sparse and more constraints must be taken into consideration, such as continuous actions, limited observations and the scalability of the policy model. In our work, we addressed this challenging CTS problem for a visual drone swarm with only local visual perception, their own state and limited egocentric observations. The scalability of the policy model is achieved by introducing only a relative position measurement with the shortest distance as the egocentric observation.

III. PRELIMINARIES

A. Quadrotor Drone Dynamics

The translational and rotational dynamics of a 6 degree-of-freedom (DOF) quadrotor of mass m can be described as follows, regardless of the wind disturbance and the aerodynamic drag:

$$\dot{\mathbf{p}}_W = \mathbf{v}_W \quad (1a)$$

$$\dot{\mathbf{v}}_W = \mathbf{R}_B^W(\mathbf{q}_{WB}) \odot \mathbf{f} + \mathbf{g} \quad (1b)$$

$$\dot{\mathbf{q}}_{WB} = \frac{1}{2} \boldsymbol{\Omega}(\boldsymbol{\omega}_B) \mathbf{q}_{WB} \quad (1c)$$

where, $\mathbf{p}_W = [x, y, z]^T$ and $\mathbf{v}_W = [v_x, v_y, v_z]^T$ are the position and translational velocity vectors of the quadrotor in the world inertial frame O_W , where the z axis of the world frame is aligned with the direction of the gravity \mathbf{g} . $\mathbf{q}_{WB} = [q_0, q_1, q_2, q_3]^T$ denotes a unit quaternion which is used to represent the quadrotor's attitude, while $\boldsymbol{\omega}_B = [\omega_x, \omega_y, \omega_z]^T$ denotes the body angular velocity (roll, pitch, and yaw respectively) in the body frame O_B . \mathbf{R}_B^W defines the transform matrix from the body frame O_B to the world inertial frame O_W , and it is a function of \mathbf{q}_{WB} . $\mathbf{f} = [0, 0, f]^T$ is the

mass-normalized thrust vector, with $f = \sum_{i=1}^4 f_i^B/m$ and $\mathbf{g} = [0, 0, -g_z]^T$ with $g_z = 9.81m/s^2$ being the gravity acceleration on Earth. We denote the $\boldsymbol{\Omega}(\boldsymbol{\omega}_B)$ as the skew-symmetric matrix and is given by

$$\boldsymbol{\Omega}(\boldsymbol{\omega}_B) = \begin{bmatrix} 0 & -\omega_x & -\omega_y & -\omega_z \\ \omega_x & 0 & \omega_z & -\omega_y \\ \omega_y & -\omega_z & 0 & \omega_x \\ \omega_z & \omega_y & -\omega_x & 0 \end{bmatrix} \quad (2)$$

Vector $\mathbf{x} = [\mathbf{p}_W, \mathbf{v}_W, \mathbf{q}_{WB}]^T$ and $\mathbf{u} = [f, \omega_x, \omega_y, \omega_z]^T$ are selected as the states and the control inputs of a quadrotor respectively. The body's momentum will not be examined because deployed high-bandwidth controllers can precisely track the angular rate commands, allowing angular dynamics to be ignored.

B. Multi-agent Reinforcement Learning

Reinforcement Learning (RL) is a technique for mapping the state space to the action space in order to maximize a long-term return with given rewards. The learner is not explicitly told what action to carry out but must figure out which action will yield the highest reward during the exploring process. We can describe the multi-agent reinforcement learning in our CTS problem as a multi-agent Finite Markov Decision Processes (FMDPs) [31] which is defined by a tuple $\langle \mathcal{S}, \{\mathcal{O}^n\}, \{\mathcal{A}^n\}, \mathcal{P}, \mathcal{R}, \mathcal{G}, N, d_0, \gamma \rangle$ with N agents denoted by $n \in [N]$. Since there is no knowledge of the target in our work, goal signals \mathcal{G} can be ignored in the following description. We denote $t \in \mathbb{N}_{\geq 0}$ as the time step, where $\mathbb{N}_{\geq 0}$ is the natural numbers. At time step t and global state $s_t \in \mathcal{S}$, each agent n obtains an observation $o_t^n := o^n(s_t) \in \mathcal{O}^n$, and take an action $a_t^n \in \mathcal{A}^n$. $\mathcal{P}(s_{t+1} | s_t, \mathbf{a}_t) : \mathcal{S} \times \mathcal{A} \times \mathcal{S} \mapsto [0, 1]$ is the transition probability for the environment moves from the current state s_t to the next state s_{t+1} with joint action $\mathbf{a}_t := \{a_t^1, \dots, a_t^N\}$. \mathcal{R} refers to the set of possible rewards, with $\mathcal{R} \subseteq \mathbb{R} \cup \{-\infty, \infty\}$. Furthermore, the reward at time t is \mathcal{R}_t and elements of the reward set are denoted by r while the infimum and supremum are r_{\min} and r_{\max} respectively. Each agent will receive an instantaneous reward $\mathcal{R}_t^n := \mathcal{R}(s_t, a_t^n)$ at each time step.

The agents start to learn from a global state s_0 sampled from an initial states distribution $d_0 : \mathcal{S} \mapsto [0, 1]$. At each time step t , joint actions \mathbf{a}_t are taken under a joint stochastic policy $\boldsymbol{\pi}(\mathbf{a}_t | s_t) := \prod_{n=1}^N \pi^n(a_t^n | o_t^n)$ and all agents transition to state s_{t+1} with the transition probability $\mathcal{P}(s_{t+1} | s_t, \mathbf{a}_t)$, receiving an instantaneous numerical reward \mathcal{R}_t . The objective of the MARL is to find a decentralized policy $\pi^n(a_t^n | o_t^n) : \mathcal{O}^n \times \mathcal{A}^n \mapsto [0, 1]$ to maximize the cumulative reward along an action trajectory τ^n via adjusting the weights $\boldsymbol{\theta}$ of the parametrized policy $\pi_{\boldsymbol{\theta}}^n$ over finite time steps (a training episode). The objective function can be described as a Bellman function as follows:

$$\mathcal{J}(\boldsymbol{\pi}_{\boldsymbol{\theta}}) := \mathbb{E}_{\tau^n \sim \boldsymbol{\pi}} \left[\sum_{t=0}^{t=T} \gamma^t \sum_{n=1}^N \mathcal{R}_t^n | s_0, a_0 \right] \quad (3)$$

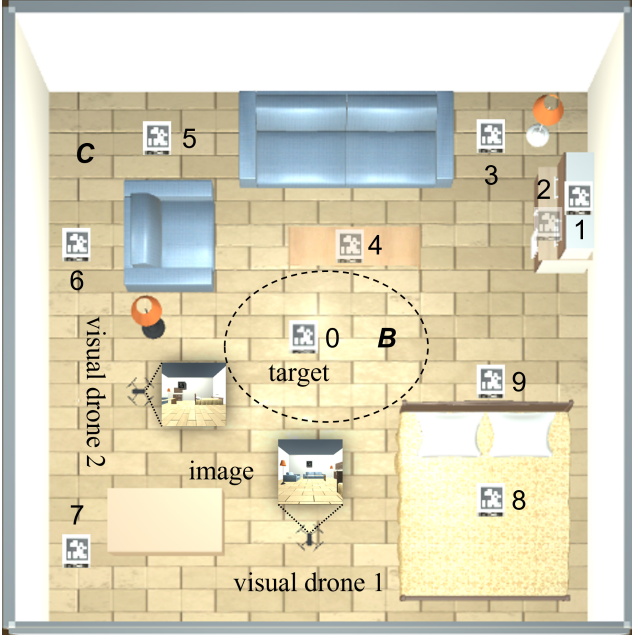


Fig. 2. A bird's-eye view of the base environment which consists of visual drone agents, obstacles and a target. The furniture objects are the obstacles such as sofas, the bed and tables; The cubic textured with April Tag is the target that drone agents need to find and reach. Each object is bounded by a collider for collision detection. Target can spawn in a closed sphere set B which is easily seen, or a discrete set C consists of several hidden locations marked with numbers 1 – 9.

where $\gamma \in [0, 1)$ is the discount-rate parameter and T is the final time step of an episode. The joint optimal policy is obtained by:

$$\pi_{\theta}^* = \underset{\pi}{\operatorname{argmax}} \mathcal{J}(\pi_{\theta}) \quad (4)$$

IV. METHODOLOGY

A. Problem Formulation

In this section, the collaborative task search problem is formulated into a multi-agent reinforcement learning problem. The agent n is referred as the visual drone in this paper. Our goal is to learn a decentralized optimal stochastic policy $\pi_{\theta}^{n*} \in \pi_{\theta}^*$ for a drone swarm (a collaborative team) with N agents to quickly find and navigate towards a hidden target denoted by g and avoid collisions (can be formulated by rewards \mathcal{R}) using only raw images, own dynamic states and egocentric measurements as observations \mathcal{O}^n . There is no prior knowledge of the target g , and the only connection between each drone is the range sensor, from which the drone can obtain the relative positions of other agents in its view. During the inference process, each drone agent continues to take actions based on the policy distribution until the target is reached.

1) *Environment Setup*: To train and evaluate the agents, a high-fidelity simulation environment is required in which we can add customized objects, such as obstacles, agents and sensors to represent the global states \mathcal{S} . We build our simulation environment using Unity rendering engine¹ which

allows us to generalize our model into different scenarios. The simulation scenarios become increasingly complex over different training stages. However, the simulation's base environment, which contains the agent drones and objects, is largely unchanged. Fig. 2 shows a base environment which consists of drone agents, obstacles and a box target. More complex environments can be generated by enlarging the size of the rooms, adding more obstacles and hiding the target at a corner where the drone agents can hardly find.

The target can be spawned randomly within a closed sphere set $B(ct, rd)$, in which the drone can easily detect at first sight. ct and rd are the center point and the radius of the sphere, respectively. Otherwise, it will be randomly placed at a predefined hidden corner drawn from a discrete set $C(n_{loc})$ which is hidden from the first sight. n_{loc} is the size of C , i.e., the number of hidden locations chosen. For instance, we can choose these locations with $n_{loc} = 5$, namely, under the desk, behind the couch, below the cupboard, below the lamp and above the cupboard. The probability of spawning a target at different locations is controlled by the spawning probability threshold ϵ . A random value r_{seed} within interval $[0, 1)$ is generated when each episode begins. If r_{seed} is greater than ϵ , the target will be spawned in B , otherwise, it will be hidden at a place of C . The probability density function (pdf) of spawning a target can be described as:

$$Pr(target) = \begin{cases} U(B), & r_{seed} > \epsilon \\ U(C), & r_{seed} \leq \epsilon; \end{cases} \quad (5)$$

, where $U(\cdot)$ is a uniform distribution among a set.

The spawning probability threshold $\epsilon \in [0, 1]$ will be adaptively adjusted in a curriculum learning way in each stage to make the task more challenging for drone agents. The validity of spawning positions will be checked, where if the target's shape is overlapped with other objects, the position is regarded as invalid, and the target will be spawned again.

The components of each obstacle are outlined by Unity's mesh collider, which allows for the detection of collisions with another collider. The drone agent is modeled as a visual quadrotor equipped with a monocular RGB camera in front of the drone. The image raw of fixed pixel size obtained from the forward camera can be used for recognizing the target and navigating towards the target. If the drone agent collides with the obstacles, other agents or the target, a penalty (negative reward value) will be imposed.

2) *Observation Space*: The agent must decide which action to take based on the current observations o_t^n to maximize the rewards. The drone agent receives observation information from an onboard camera and drone's state sensors, such as IMU and positioning device. The image observation, the self state observation and egocentric observation are denoted as $o_{I,t}^n$, $o_{S,t}^n$ and $o_{E,t}^n$, respectively. The RGB image raw from the camera is down-sampled to a fixed resolution $3 \times 224 \times 224$ image $I_t \in 3 \times \mathbb{R}^{224} \times \mathbb{R}^{224}$ at every time step. The agent n knows its own translational and rotational states, i.e., local position $p_{W,n}$ and rotational quaternion $q_{WB,n}$, and the relative positions of other team agents $p_{W,nj}$, where $j \in [N]^{-n}$. However, only the relative position with the shortest distance p_{W,nj^*} , i.e., $\|p_{W,nj^*}\| = \min(\|p_{W,nj}\|)$ for $j \in [N]^{-n}$,

¹<https://unity.com/>

is considered as the input observation of the policy model. Besides, a normalized forward direction vector $\bar{\mathbf{d}}_W \in \mathbb{R}^3$ is included in the observation space to make sure the drone agent senses the direction. To ensure smooth maneuvering for the drone, the last action $\mathbf{a}_{t-1}^n \in \mathbb{R}^4$ is also stored as an observation.

For each drone, only the current RGB image I_t^n are used and encoded into a vector $\mathbf{o}_{EV,t}^n \in \mathbb{R}^{512}$ with a Convolutional Neural Network (CNN). This CNN allows the drone to detect different objects in their environment, such as obstacles, team agents and the target, and sense the depth information. The concatenated observation vector for the drone n at time step t is $\mathbf{o}_t^n = [\mathbf{o}_{EV,t}^n, \mathbf{p}_{W,t}, \mathbf{q}_{WB,t}, \bar{\mathbf{d}}_{W,t}, \mathbf{a}_{t-1}^n, \mathbf{p}_{W,nj^*,t}] \in \mathbb{R}^{529}$.

3) *Action Space*: In this work, we only concentrate on the high-level controller for drones. The low-level controller inside the drone tries to keep track of the high-level commands via inputs \mathbf{u} . Since the quadrotor is an under-actuated system, the selected high-level commands (actions \mathbf{a}_t^n) are the four velocity commands generally used in the mobile Robot Operation System (ROS), i.e., the desired velocity of quadrotor in the body frame O_B , namely $\hat{v}_x^B, \hat{v}_y^B, \hat{v}_z^B$ and $\hat{\omega}_z^B$. The action space \mathcal{A}^n consists of these four continuous actions that drive the drones to fly towards the target while exploring the constrained 3D space.

4) *Reward Function*: The reward function consists of two parts: one is the existential penalty $\mathcal{R}_P = -t/T_{max}$ of the team, where T_{max} is the allowable time steps in an episode, while the other is the terminal reward \mathcal{R}_T . The existential penalty serves to accelerate the exploring progress, and the terminal reward serves to guide the drone to fly towards the target with the correct forward direction and to avoid crash simultaneously.

The terminal reward is a set function described as:

$$\mathcal{R}_T = \begin{cases} +5, & \text{if agent reaches the target} \\ r_C, & \text{if agent crashes} \end{cases} \quad (6)$$

Where r_C is the penalty when the drone collide with the obstacles or other agents.

$$r_C = -\alpha \frac{\|\mathbf{d}_T\|}{\|\mathbf{d}_{init}\|} - \frac{\beta}{\pi} \arccos \frac{\langle \mathbf{d}_T, \bar{\mathbf{d}}_W \rangle}{\|\mathbf{d}_T\| \cdot \|\bar{\mathbf{d}}_W\|} - 3 \quad (7)$$

where, \mathbf{d}_T is the vector from the collision position to the target position and \mathbf{d}_{init} is the vector from the initial position to the target position; $\|\cdot\|$ denotes the norm of the vector and $\langle \cdot \rangle$ is the inner product of two vectors; α and β are the weights to adjust the penalty from the distance to fly and the penalty caused by the forward direction. Note that the terminal reward r_C is accounted for each agent, and the episode terminates only when all agents crash, while the positive reward +5 is a team reward, i.e., when the episode ends, each agent receives +5 if one agent can reach the target.

B. Network Architecture

As shown in Fig. 3, the neural network used in this paper consists of 3 parts: the image encoder, the policy network and the memory network. The memory network is embedded into the policy network for processing the temporal sequence observations. We have conducted performance analysis for 3

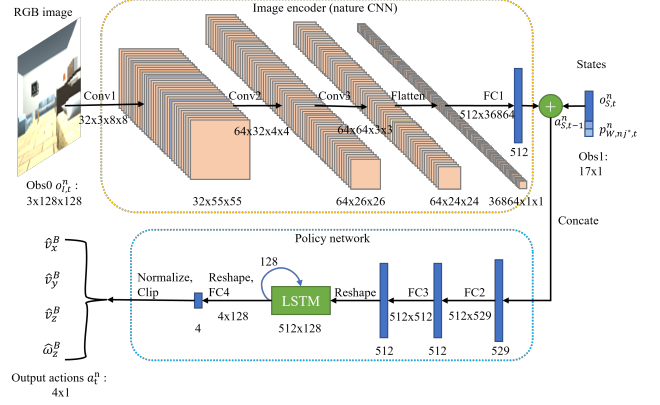


Fig. 3. Illustration of the neural network architecture for target search, which consists of the image encoder, the policy network and the memory network.

visual encoders, namely simple 2-layers CNN, nature CNN [11] and ResNet [32]. Considering the efficiency and search performance, a shallow neural network-nature CNN is used in our model. The image encoder-nature CNN consists of 3 convolutional layers, 1 flatten layer and 1 fully connected layer. A Leaky Rectified Linear Unit (Leaky ReLU) is adopted as the activation function for all convolutional layers and the encoder's fully connected (FC) layer. The image encoder turns the RGB image of fixed resolution into a 512 dimensional flattened vector. The policy neural network is designed with 2 FC (512-nodes with a Sigmoid activation function) layers which maps the concatenated observation vector $\mathbf{o}_t^n \in \mathbb{R}^{529}$ into a continuous action vector $\mathbf{a}_t^n \in \mathbb{R}^4$. The memory network-Long Short Term Memory (LSTM) [33] is a recurrent neural network used to feedback previous outputs and generate smooth trajectories for drones.

C. Adaptive Curriculum Embedded Multi-stage Learning

1) *Adaptive Embedded Curriculum (AEC)*: In the standard curriculum learning methods [17], [34], the curriculum is manually designed with a static, discrete parameter sequence in which the task difficulty level is progressively increased with a pre-designed mode. Even though the pre-designed curriculum parameter can be post-adjusted according to the training results, it is inconvenient and inefficient to obtain a satisfactory curriculum. Hence, it is hard for agents to achieve their best performance. In contrast to the standard curriculum learning methods, based on the ACMSL, the task difficulty level is adaptively adjusted with a changing rate δ_ϵ based on the success rate of finding the target achieved by agents. If the success rate rises to a high boundary sr_h , the task difficulty level increases. Correspondingly, if the success rate drops to a low boundary sr_l , the task difficulty level decreases. There are several parameters that can be considered to derive the task difficulty level, such as the size of the space, the number of obstacles, the size of the target, and the spawning probability threshold (ϵ) in (5). In our scenario, the task difficulty level is formulated by the spawning probability threshold since our main goal is to find the hidden target as fast as possible. In the following discussion, the task difficulty level is denoted by ϵ .

Other parameters can be adjusted in the domain randomization. The AEC based on the spawning probability threshold is described in Algorithm 1.

Algorithm 1: Adaptive Embedded Curriculum (AEC)

Input: An initial task difficulty level ϵ_0 , changing rate $\delta_\epsilon, sr_l, sr_h$

Output: The spawning position \mathbf{p}_{goal} of target

```

1 On the start of training:
2 Initialize  $\mathbf{p}_{W,0}, \mathbf{v}_{W,0}, \mathbf{q}_{WB,0}, successRate = 0.0,$ 
    $successCount = 0, episodeCount = 0$  ;
3 On each episode begin:
4 if  $episodeCount \neq 0$  then
5    $successRate \leftarrow successCount / episodeCount$ ;
6 end
7  $episodeCount \leftarrow episodeCount + 1$ ;
8 if  $successRate > sr_h$  then
9    $\epsilon \leftarrow \max(\epsilon + \delta_\epsilon, 1.0)$ ;
10 end
11 if  $successRate < sr_l$  then
12    $\epsilon \leftarrow \min(\epsilon - \delta_\epsilon, 0.0)$ ;
13 end
14 Spawn the target according to (5);
15 On each episode end:
16 if one drone reaches the target then
17    $successCount \leftarrow successCount + 1$ ;
18 end
19 if all drones crash then
20   end the episode;
21   back to 3;
22 end

```

2) *Stage 1:* At stage 1, the objective is to train a single drone to identify, track and fly towards a randomly spawned target according to Algorithm 1. During stage 1, the drone explores the environment with the designed reward function. The MARL problem is reduced into a single agent ($N = 1$) problem, and the group reward becomes the agent n 's reward. The optimal policy achieved by agent n is the greedy policy [19]. The drone will learn to find and approach the stationary target without crashing into obstacles.

3) *Stage 2:* Once the drone has successfully learned the target-approaching behavior, another drone is added to the scene in stage 2 for generating collaborative behavior. The trained model in stage 1 is used to initialize the model in stage 2. These two drones are further trained to search the same target without crashing into each other. Once the agents crash (collide with the obstacles or other agents), their status becomes inactive until the next episode. The episode ends when all agents have crashed or one agent has reached the target.

In our training process, only the states of the agents and the image raw are collected for observations, without the need for information on relative positions between the agents and the target, which is usually the case for the traditional numerical methods [23]. Only at the end of each episode, the distance values are counted into the reward function. Meanwhile, the

TABLE I
DOMAIN RANDOMIZATION

Environment Randomization	
light intensity I_v	$U(0.2, 1.0)$
scale of target λ_{target}	$U(0.2m, 0.3m)$
yaw angle of target ψ_{target}	$U(0^\circ, 360^\circ)$
Agent Randomization	
position noise	$U(\mathbf{B}(ci, 0.2m))$
noise in yaw angle of agent	$U(-30^\circ, 30^\circ)$

existential penalty is designed to encourage the agent to reach the target as fast as possible.

The proximal policy optimization (PPO) algorithm [35] is selected for our training. Compared with Soft Actor-Critic (SAC) algorithm [36], PPO is more effective and robust for problems with a continuous action space by using “clipped” surrogate objective and on-policy learning.

D. Domain Randomization

Domain randomization [37]–[39] is an effective technique to improve the generalization capability of the model during the training and hence increase the success rate of Sim2Real [37] transfer to unseen scenarios. At the beginning of each episode, environment parameters and agents' states are randomly sampled from uniform distributions. In our work, the domain randomization used can be divided into (1) environment randomization that involves randomization of parameters, such as the light intensity in Unity scenes I_v , the scale λ_{target} and the yaw angle ψ_{target} of the target; (2) agent randomization that involves randomization of parameters, such as the initial states of agents. The environment randomization extends the trained model to accomplish the tasks in unseen scenarios while the agent randomization enables the agents to start with perturbations in their initial configurations.

As listed in Table I, the environment parameters are randomly sampled from an uniform distribution $U(min, max)$ while the agent randomization is generated by adding a random noise from an uniform distribution $U(\cdot)$. Note that the position noise of agent is sampled from an uniformly distributed closed sphere set $\mathbf{B}(ci, ri)$, i.e., $U(\mathbf{B}(ci, ri))$, where ci is the initial position of agents and ri is the radius of sphere set. $U(min, max)$ and $U(\mathbf{B}(ci, ri))$ are generated via the *Random.Range(min, max)* function and *Random.insideUnitSphere * ri* operator in Unity respectively.

V. EXPERIMENTS AND RESULTS

In this section, we present the simulation experiments, including the training process and inference tests, and the physical experiments covering the model Sim2Real transfer and the real-time flight tests. The architecture of simulation and physical experiment platform is illustrated in Fig. 4, which consists of a simulation workstation (with AMD Ryzen 9 5900X 12 cores CPU, Nvidia RTX 3090 Gaming OC 24GB GPU and 32GB RAM), a laptop computing center, the OptiTrack motion capture server streaming the position data of selected rigid bodies and a Tello Edu visual drone swarm.

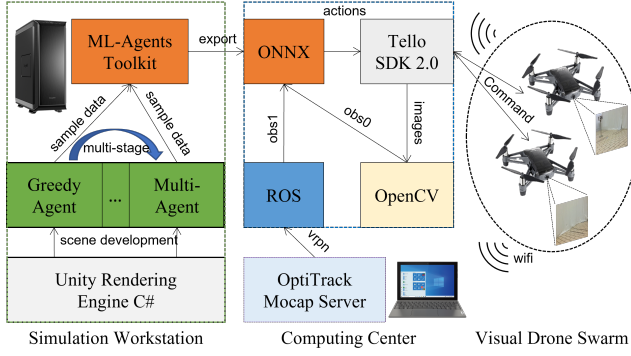


Fig. 4. Illustration of the training and experiment framework.

TABLE II
HYPERPARAMETERS USED FOR PPO TRAINING

Parameter	Value	Parameter	Value
batch size	2048	buffer size	10240
learning rate	0.0003	beta	0.01
epsilon ϵ	0.2	lambda λ	0.95
number of epochs	3	learning rate schedule	linear
checkpoints	10	maximum steps	12000000

The simulation workstation is used to develop simulation environments for training and testing and export the trained neural network model for deployment. With the trained ONNX² model, the computing center acquires real-time observations from the motion capture server and Tello Edu drones, and generates corresponding actions which drive the Tello Edu visual drones to search the target via Tello SDK 2.0³. The computing center is connected to the OptiTrack motion capture system to subscribe the position data of drones via Robots Operation System (ROS) nodes. The image observation is acquired from the onboard camera of Tello Edu drones using necessary image processing. Note that the Tello Edu drone can only be set as a wireless access point (AP) to stream the video. Hence, multiple USB WIFI adapters are used in the computing center for connecting to the drones via WIFI separately.

A. Simulation Experiments

1) *Settings*: Our simulation platform is developed based on the Unity rendering engine and ML-Agents Toolkit [34], which is a flexible simulation and training platform for multi-agent reinforcement learning. Scenes of target search with a single greedy agent and CTS with a drone swarm are developed successively. The dimensions of the base simulation environment in Fig. 2 is $5m \times 5m \times 3m$ (width \times length \times height). In the AEC, the task difficulty level starts from $\epsilon_0 = 0.1$ and changes with $\delta_\epsilon = 0.1$. Success rate boundaries are set to $sr_h = 0.90$ and $sr_l = 0.20$. Allowed maximum time step is $T_{max} = 5000$ in one episode. Reward weights are $\alpha = 1$ and $\beta = 0.1$. The initial linear and angular velocity of drones are reset to zero at the start of each episode.

²<https://onnx.ai/>

³<https://www.ryzero.com/tello-edu/downloads>

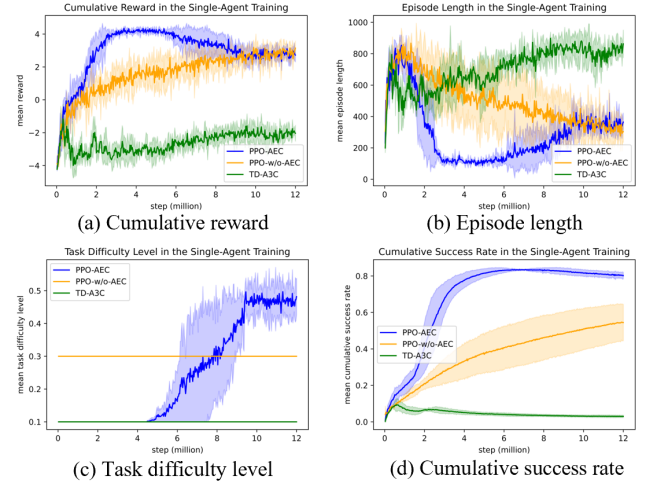


Fig. 5. Learning curves of the PPO-AEC (ours), the baseline TD-A3C and the ablation PPO-w/o-AEC in the single-agent training. Mean and standard deviation (shaded) over 3 independent runs conducted every 12 million training steps (episodes).

2) *Baselines and Ablations*: The performance of our approach is compared against TD-A3C [14], which only uses visual observations, and CM3 [19], which is trained without an AEC (with a fixed task difficulty level $\epsilon = 0.3$). We ensure that TD-A3C and CM3 are modified such that both of them can be applied for the target search tasks in the training. Since TD-A3C is proposed to address a single agent navigation problem, we evaluate its performance with our PPO with AEC (PPO-AEC) and PPO without AEC (PPO-w/o-AEC) in the single-agent training.

To study the data-efficiency of the proposed multi-stage method, fully trained stage 2 (labeled as Direct) and ACMSL are compared together with CM3 in the multi-agent training. Stage 1 of ACMSL and CM3 are the same, trained for 3 million steps with the AEC. For fair evaluation, we also trained TD-A3C and CM3 with the PPO algorithm since we consider the method frameworks not the training algorithm itself. The hyperparameters of PPO for all training remain the same.

3) *Training*: The hyperparameters of the PPO training are listed in Table II. The training tools version are ml-agents-toolkit: 0.27.0; ml-agents-envs: 0.27.0; communicator API: 1.5.0; PyTorch: 1.8.2+cu11.1. To accelerate the training process, 6 copies of the environment are placed in one scene, and 3 concurrent Unity instances are invoked at the start of training. The mean and the standard of deviation values over 3 runs of the single-agent training are illustrated in Fig. 5. From results shown in Fig. 5, the PPO-AEC achieves the best performance compared to PPO-w/o-AEC and TD-A3C based on the cumulative success rate and the episode length, even at a higher task difficulty level. It verifies the data efficiency and effectiveness of the proposed AEC. TD-AEC obtains the least satisfactory performance as the agent can hardly find the target even at the easiest task level, which illustrates the drawbacks of the targeted-driven navigation with purely visual perception for target search.

For the multi-agent training, the stage 2 training are ini-

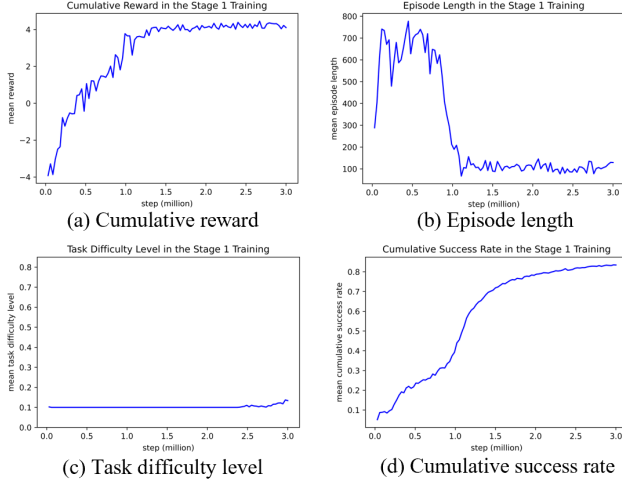


Fig. 6. Stage 1 training curves for ACESML and CM3 with single-agent over 3 million steps (episodes).

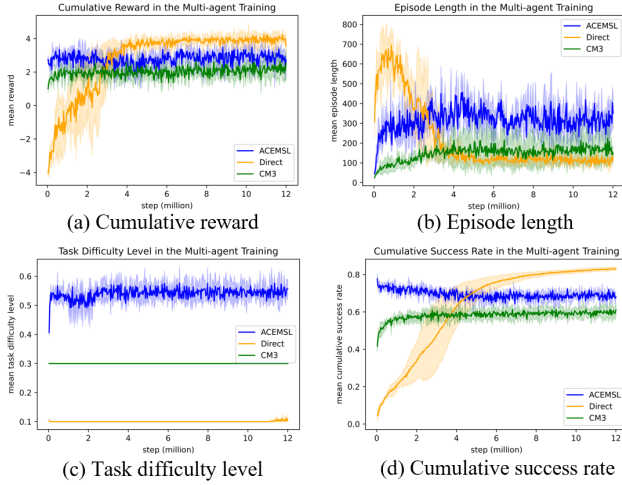


Fig. 7. Learning curves of the ACESML (ours), the baseline CM3 and the ablation “Direct” in the multi-agent training. Mean and standard deviation (shaded) over 3 independent runs conducted every 12 million training steps (episodes).

tialized from the existing model of stage 1 training over 3 million steps. The results of stage 1 training are shown in Fig. 6. The mean values with the standard deviation over 3 runs of the multi-agent training are illustrated in Fig. 7. With the assistance of stage 1, ACESML and CM3 converge more than 1 million steps (3 million steps in the stage 1 training) faster than the “Direct” method (see Fig. 7 (a)), which demonstrates the significant data-efficiency of the multi-stage learning. Compared to CM3, ACESML benefits significantly from the adaptive embedded curriculum as ACESML achieves a higher cumulative reward and success rate even with higher task difficulty levels (see Fig. 7 (c)). The AEC can fully liberate the advantages of multi-stage learning for the target search task with a visual drone swarm.

As indicated in the single-agent and multi-agent training, the proposed ACESML addressed the challenges of the 3D sparse continuous space exploration and the collaborative

TABLE III
TARGET SEARCH PERFORMANCE (SUCCESS RATE % / MEAN TIME STEPS TO REACH) ON VARIOUS ROOM DIMENSIONS

Room Dimensions (m)	$5 \times 5 \times 3$	$8 \times 8 \times 3$	$10 \times 10 \times 3$
1 drone	75.4% / 162	52.8% / 301	16.0% / 325
2 drones	79.3% / 107	61.1% / 236	35.9% / 256
3 drones	63.8% / 104	62.0% / 178	41.9 % / 254

behavior requirement for multi-agent systems. It combines the advantages of adaptive curriculum learning and multi-stage learning to significantly improves over data efficiency in the training.

4) *Testing*: We tested our models from single agent training and multi-agent training on various room dimensions with 500 episodes evaluated per experiment, where the task difficulty level is set as $\epsilon = 0.3$. We also demonstrated the scalability of the trained model with ACESML, where multiple drones are spawned at the start area. The success rate and the mean time steps to reach with a different number of drones on various room dimensions are listed in Table III. As the room dimensions increase, the success rate drops, and the required time steps to reach the target increase as well. On the other hand, deploying more drones helps increase the success rate and reduce the required time steps to reach the target, which illustrates the advantages of using a visual drone swarm for target search. However, the scale of the swarm is constrained by the size of the room (the success rate drops from 75.4% to 63.8% in Table III when 3 drones are deployed in the room of $5m \times 5m \times 3m$) since there is a higher chance of the drones crashing into one another if too many drones are flying within a small room.

B. Physical Experiments

To evaluate the trained models’ generalization and Sim2Real capability, we transfer our models to an unseen large indoor environment without fine-tuning, and their performance on different devices is compared. The test environment is an enclosed room with the size of $8m \times 7m \times 4m$. Each side, excluding the floor and the ceiling of the environment, is covered by white curtains. The target is a parcel box with the size of $0.20m \times 0.30m \times 0.20m$, placed randomly on/behind obstacles within the environment at several testing positions. Every side of the box is attached with a printed April Tag (Tag36h11) [40]. An OptiTrack motion capture system with eight cameras is used for broadcasting positions of the drone(s) and the target. The position of the target is used to detect if the drones can achieve their goal. In our experiment, the laptop computing center and Tello Edu drones are used to deploy our trained models and conduct flight tests. In addition, for deployment on the onboard computers, three of the following computing platforms are evaluated on their performance in terms of the execution speed of the trained model using only their CPUs. Note that the trained model for only a single drone deployment is considered for this evaluation.

- Lenovo Ideapad Slim 5 Pro laptop running Ubuntu OS with AMD Ryzen 7 5800H CPU and 16GB DDR4 RAM.

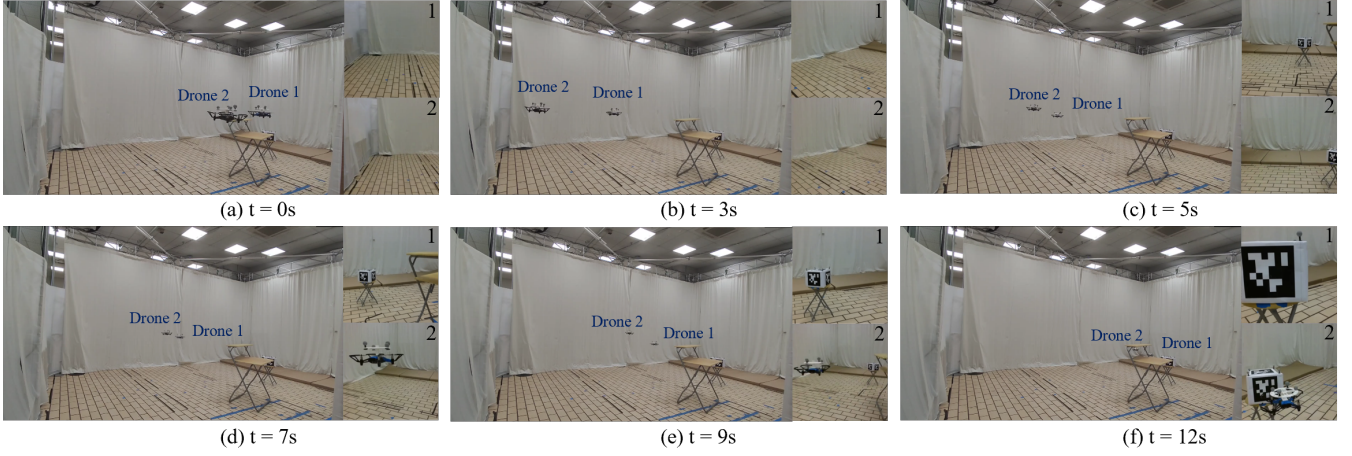


Fig. 8. The snapshots of a visual drone swarm when perform the CTS. The images perceived by the cameras of drone 1 and drone 2 are labeled as 1 and 2 respectively at the right side of each snapshot.

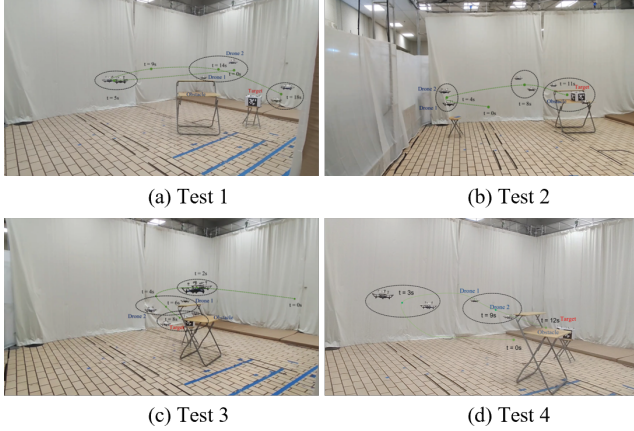


Fig. 9. The trajectories of a visual drone swarm successfully performing the CTS in four tests with different initial conditions.

- NVIDIA Jetson Xavier NX running Ubuntu OS with 6-core NVIDIA Carmel 64-bit CPU and 8GB RAM.
- Raspberry Pi 4 Model B with 64-bit ARM Cortex-A72 (ARMv8) and 8GB RAM.

All of these devices use Python3 and ONNXRuntime⁴ for inference with the trained model in ONNX format. PyTorch and Torchvision are used for data processing on all of the devices. Table IV illustrates the execution speed of the trained model in the unit of frames per second (fps).

Real-time processing capability is crucial for model deployment on computing devices. The evaluation criterion for device performance is set such that for any device that has real-time processing capability for neural network models, it should be able to execute every part of the trained model, including the data pre-processing step, with the speed of at least 20 frames per second (fps). According to the result in Table IV, only NVIDIA Jetson Xavier NX and Lenovo Ideapad Slim 5 laptop meet the evaluation criterion; therefore, these devices have real-time processing capability. However,

TABLE IV
COMPUTING PERFORMANCE OF DEVICES

Devices	Raspberry Pi	Xavier NX	Laptop
Program Component			
Image Processing (ms)	85.1 ± 3.8	35.9 ± 0.6	16.1 ± 0.6
ONNX Model (ms)	48.2 ± 2.8	10.5 ± 0.4	4.47 ± 0.49
Control Commands (ms)	3.08 ± 0.75	1.62 ± 0.15	0.35 ± 0.03
All Process (ms)	128 ± 7	48.1 ± 0.9	19.8 ± 0.6
(fps)	8.15 ± 0.33	20.9 ± 0.4	51.2 ± 1.3

the Raspberry Pi execution speed is too low to be considered as real-time processing. As the experiment evaluated only on the performance using CPU, the performance of NVIDIA Jetson Xavier NX and Lenovo Ideapad Slim 5 laptop can be improved further using GPUs, parallel computing with CUDA⁵, and deep learning accelerators, such as TensorRT⁶.

Each drone is set as a wireless AP connected with the computing center during real-time flight tests. As every Tello Edu drone has a similar, immutable IP address (192.168.10.1) on its network, there is an IP address conflict issue when all drones are connected with the same computer. To resolve, network routing is required to route drones' network to different virtual IP addresses perceived by the computer via docker services⁷.

The drones stream the video data captured by their cameras to the laptop computing center via WIFI. PyAV library⁸ is imported to open and decode drones' video stream into image frames with a size of $3 \times 720 \times 960$ recognized by Torchvision. Considering the mismatch between the aspect ratios of the raw images and the model training input, the image frames are firstly cropped to $3 \times 720 \times 720$ around the image center. Thenceforth, Torchvision reshapes and converts the cropped images separately to a NumPy array of $3 \times 224 \times 224$, consistent with the size of visual observation in the trained

⁴<https://onnxruntime.ai/>

⁵<https://developer.nvidia.com/cuda-zone>

⁶<https://developer.nvidia.com/tensorrt>

⁷<https://www.docker.com/>

⁸<https://github.com/PyAV-Org/PyAV>

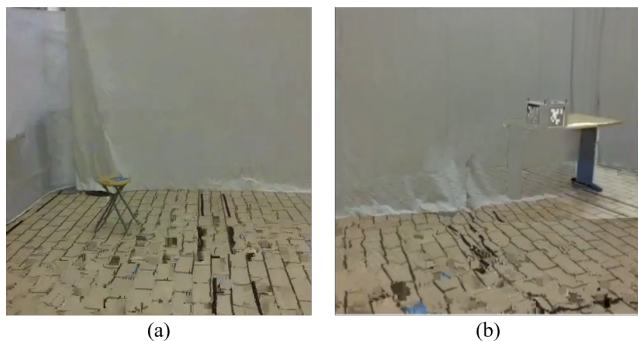


Fig. 10. Image blurry and loss of video stream cause the failure of task. (a) Obstacle blurry; (b) Target blurry

model. The model generates translational and angular velocity commands in a loop block based on the obtained visual data and drone's position published by the motion capture system. These velocity commands drive the connected drones to search and reach the target collaboratively in real-time (see Fig. 8). More details can be found in the video: <https://youtu.be/LuCK97i5Bcw> and the code: <https://github.com/NTU-UAVG/collaborative-target-search-vision-drone-swarm.git>.

In this work, we conduct 25 tests each for the single drone and collaborative two drones target search to evaluate the target search performance in an unseen physical environment using the trained models. This evaluation focuses on the success rate and the time taken to reach the target. The experiments for the single drone and collaborative two drone target search use different models from the single-agent training and the multi-agent training accordingly. During the tests, the drones are placed at the start area with random forward directions and positions. The outcome of such test is considered a success when a drone reaches the target and lands within 0.5 m horizontal distance from the target, otherwise is considered a failure. The trajectories of several success cases are illustrated in Fig. 9.

The target search performance using a single drone and collaborative two drones in the first and second physical experiment are compared and shown in Table V. The result shows that the CTS displays a higher performance in terms of time to reach the target and the success rate (64% for two drones while 48% for a single drone). Therefore, the collaboration of drones for target search helps to find the target faster and more accurately. Meanwhile, the success rate illustrated in the physical experiments is very close to that of the simulations as indicated in Table III, which demonstrates the generalization and the Sim2Real capability of trained models.

Some of the failure cases could be attributed to the video blur similar to Fig. 10, which gives wrong information to the trained model, so the velocity commands are inaccurate.

VI. CONCLUSION

This paper proposed a data-efficient reinforcement learning-based approach, Adaptive Curriculum Embedded Multi-Stage Learning (ACEMSL), to address the challenges of CTS with

TABLE V
TARGET SEARCH PERFORMANCE IN REAL TIME FLIGHT

Experiment	Single Drone	Two Drones (Collaborative)
Success Rate	48%	64%
Time to Target (second)	12.9 ± 0.8	12.2 ± 0.8
(step)	143 ± 10	142 ± 13

a visual drone swarm. Our approach improves over the standard curriculum learning via adopting the designed AEC and combining the multi-stage learning to achieve the 3D sparse reward space exploration and collaborative behaviors among a visual drone swarm. Without prior knowledge of the target, the drone swarm performs CTS with only local visual perception and egocentric observations.

The training results show that our proposed approach outperforms the state-of-the-art direct reinforcement learning methods and the multi-stage learning-CM3 in terms of training time and success rate. We also demonstrated the generalization and Sim2Real capability of our trained models in the real-time flight experiments conducted in an unseen physical environment. The experiment results verified the effectiveness of a drone swarm for CTS based on the metrics of success rate and time to reach. To the best of our knowledge, this work is unprecedented in achieving and demonstrating the CTS with a visual drone swarm in real life.

Our results motivate future work to evaluate and alleviate the effects of CTS performance caused by communication loss and cyber attacks on visual perception.

ACKNOWLEDGMENT

The authors would like to thank Chun Wayne Lee and Yi Hong Ng (Nanyang Technological University, Singapore) for their help or valuable feedback on this work.

REFERENCES

- [1] E. T. Alotaibi, S. S. Alqefari, and A. Koubaa, "Lsar: Multi-uav collaboration for search and rescue missions," *IEEE Access*, vol. 7, pp. 55 817–55 832, 2019.
- [2] S. Hayat, E. Yanmaz, T. X. Brown, and C. Bettstetter, "Multi-objective uav path planning for search and rescue," in *2017 IEEE International Conference on Robotics and Automation (ICRA)*, 2017, pp. 5569–5574.
- [3] Z. Chen, J. Alonso-Mora, X. Bai, D. D. Harabor, and P. J. Stuckey, "Integrated task assignment and path planning for capacitated multi-agent pickup and delivery," *IEEE Robotics and Automation Letters*, vol. 6, no. 3, pp. 5816–5823, 2021.
- [4] D. Câmara, "Cavalry to the rescue: Drones fleet to help rescuers operations over disasters scenarios," in *2014 IEEE Conference on Antenna Measurements & Applications (CAMA)*. IEEE, 2014, pp. 1–4.
- [5] Y. Liu, J. M. Montenbruck, D. Zelazo, M. Odelga, S. Rajappa, H. H. Bühlhoff, F. Allgöwer, and A. Zell, "A distributed control approach to formation balancing and maneuvering of multiple multirotor uavs," *IEEE Transactions on Robotics*, vol. 34, no. 4, pp. 870–882, 2018.
- [6] J. Hu, H. Zhang, L. Liu, X. Zhu, C. Zhao, and Q. Pan, "Convergent multi-agent formation control with collision avoidance," *IEEE Transactions on Robotics*, vol. 36, no. 6, pp. 1805–1818, 2020.
- [7] F. Schiano and P. R. Giordano, "Bearing rigidity maintenance for formations of quadrotor uavs," in *2017 IEEE International Conference on Robotics and Automation (ICRA)*. IEEE, 2017, pp. 1467–1474.

- [8] E. Soria, F. Schiano, and D. Floreano, "Predictive control of aerial swarms in cluttered environments," *Nature Machine Intelligence*, vol. 3, no. 6, pp. 545–554, 2021.
- [9] B. P. Duisterhof, S. Li, J. Burgués, V. J. Reddi, and G. C. de Croon, "Sniffy bug: A fully autonomous swarm of gas-seeking nano quadcopters in cluttered environments," in *2021 IEEE/RSJ International Conference on Intelligent Robots and Systems (IROS)*. IEEE, 2021, pp. 9099–9106.
- [10] J. Spaethe, L. Chittka, and P. Skorupski, "Visual search and decision making in bees: time, speed and accuracy," *International Journal of Comparative Psychology*, 2006.
- [11] V. Mnih, K. Kavukcuoglu, D. Silver, A. A. Rusu, J. Veness, M. G. Bellemare, A. Graves, M. Riedmiller, A. K. Fidjeland, G. Ostrovski, S. Petersen, C. Beattie, A. Sadik, I. Antonoglou, H. King, D. Kumaran, D. Wierstra, S. Legg, and D. Hassabis, "Human-level control through deep reinforcement learning," *Nature*, vol. 518, no. 7540, pp. 529–533, feb 2015.
- [12] C. Piciarelli and G. L. Foresti, "Drone swarm patrolling with uneven coverage requirements," *IET Computer Vision*, vol. 14, no. 7, pp. 452–461, 2020.
- [13] X. Liu and Y. Tan, "Feudal latent space exploration for coordinated multi-agent reinforcement learning," *IEEE Transactions on Neural Networks and Learning Systems*, pp. 1–9, 2022.
- [14] Y. Zhu, R. Mottaghi, E. Kolve, J. J. Lim, A. Gupta, L. Fei-Fei, and A. Farhadi, "Target-driven visual navigation in indoor scenes using deep reinforcement learning," in *2017 IEEE international conference on robotics and automation (ICRA)*. IEEE, 2017, pp. 3357–3364.
- [15] P. Mirowski, R. Pascanu, F. Viola, H. Soyer, A. J. Ballard, A. Banino, M. Denil, R. Goroshin, L. Sifre, K. Kavukcuoglu, D. Kumaran, and R. Hadsell, "Learning to navigate in complex environments," *5th International Conference on Learning Representations, ICLR 2017 - Conference Track Proceedings*, 2017.
- [16] Q. Wu, X. Gong, K. Xu, D. Manocha, J. Dong, and J. Wang, "Towards Target-Driven Visual Navigation in Indoor Scenes via Generative Imitation Learning," *IEEE Robotics and Automation Letters*, vol. 6, no. 1, pp. 175–182, jan 2021.
- [17] Y. Bengio, J. Louradour, R. Collobert, and J. Weston, "Curriculum learning," in *Proceedings of the 26th annual international conference on machine learning*, 2009, pp. 41–48.
- [18] C. Xiao, P. Lu, and Q. He, "Flying through a narrow gap using end-to-end deep reinforcement learning augmented with curriculum learning and sim2real," *IEEE Transactions on Neural Networks and Learning Systems*, 2021.
- [19] J. Yang, A. Nakhaei, D. Isele, K. Fujimura, and H. Zha, "Cm3: Cooperative multi-goal multi-stage multi-agent reinforcement learning," in *International Conference on Learning Representations*, 2019.
- [20] A. D. Haumann, K. D. Listmann, and V. Willert, "DisCoverage: A new paradigm for multi-robot exploration," in *Proceedings - IEEE International Conference on Robotics and Automation*, 2010, pp. 929–934.
- [21] X. Cao, D. Zhu, and S. X. Yang, "Multi-auv target search based on bioinspired neurodynamics model in 3-d underwater environments," *IEEE transactions on neural networks and learning systems*, vol. 27, no. 11, pp. 2364–2374, 2015.
- [22] S. Hayat, E. Yanmaz, T. X. Brown, and C. Bettstetter, "Multi-objective uav path planning for search and rescue," in *2017 IEEE international conference on robotics and automation (ICRA)*. IEEE, 2017, pp. 5569–5574.
- [23] Y.-J. Zheng, Y.-C. Du, H.-F. Ling, W.-G. Sheng, and S.-Y. Chen, "Evolutionary collaborative human-uav search for escaped criminals," *IEEE Transactions on Evolutionary Computation*, vol. 24, no. 2, pp. 217–231, 2019.
- [24] C. Wu, B. Ju, Y. Wu, X. Lin, N. Xiong, G. Xu, H. Li, and X. Liang, "Uav autonomous target search based on deep reinforcement learning in complex disaster scene," *IEEE Access*, vol. 7, pp. 117 227–117 245, 2019.
- [25] Y. Song, M. Steinweg, E. Kaufmann, and D. Scaramuzza, "Autonomous drone racing with deep reinforcement learning," in *2021 IEEE/RSJ International Conference on Intelligent Robots and Systems (IROS)*. IEEE, 2021, pp. 1205–1212.
- [26] A. Loquercio, E. Kaufmann, R. Ranftl, M. Müller, V. Koltun, and D. Scaramuzza, "Learning high-speed flight in the wild," *Science Robotics*, vol. 6, no. 59, p. eabg5810, 2021.
- [27] C. Berner, G. Brockman, B. Chan, V. Cheung, P. Debiak, C. Dennison, D. Farhi, Q. Fischer, S. Hashme, C. Hesse *et al.*, "Dota 2 with large scale deep reinforcement learning," *arXiv preprint arXiv:1912.06680*, 2019.
- [28] G. Sartoretti, J. Kerr, Y. Shi, G. Wagner, T. S. Kumar, S. Koenig, and H. Choset, "Primal: Pathfinding via reinforcement and imitation multi-agent learning," *IEEE Robotics and Automation Letters*, vol. 4, no. 3, pp. 2378–2385, 2019.
- [29] Y. Liu, H. Liu, Y. Tian, and C. Sun, "Reinforcement learning based two-level control framework of uav swarm for cooperative persistent surveillance in an unknown urban area," *Aerospace Science and Technology*, vol. 98, p. 105671, 2020.
- [30] M. Damani, Z. Luo, E. Wenzel, and G. Sartoretti, "Primal _2: Pathfinding via reinforcement and imitation multi-agent learning-lifelong," *IEEE Robotics and Automation Letters*, vol. 6, no. 2, pp. 2666–2673, 2021.
- [31] R. S. Sutton and A. G. Barto, *Reinforcement learning: An introduction*. MIT press, 2018.
- [32] L. Espeholt, H. Soyer, R. Munos, K. Simonyan, V. Mnih, T. Ward, Y. Doron, V. Firoiu, T. Harley, I. Dunning *et al.*, "Impala: Scalable distributed deep-rl with importance weighted actor-learner architectures," in *International Conference on Machine Learning*. PMLR, 2018, pp. 1407–1416.
- [33] S. Hochreiter and J. Schmidhuber, "Long Short-Term Memory," *Neural Computation*, vol. 9, no. 8, pp. 1735–1780, nov 1997.
- [34] A. Juliani, V.-P. Berges, E. Teng, A. Cohen, J. Harper, C. Elion, C. Goy, Y. Gao, H. Henry, M. Mattar *et al.*, "Unity: A general platform for intelligent agents," *arXiv preprint arXiv:1809.02627*, 2018.
- [35] J. Schulman, F. Wolski, P. Dhariwal, A. Radford, and O. Klimov, "Proximal policy optimization algorithms," *arXiv preprint arXiv:1707.06347*, 2017.
- [36] T. Haarnoja, A. Zhou, P. Abbeel, and S. Levine, "Soft actor-critic: Off-policy maximum entropy deep reinforcement learning with a stochastic actor," in *International conference on machine learning*. PMLR, 2018, pp. 1861–1870.
- [37] J. Tobin, R. Fong, A. Ray, J. Schneider, W. Zaremba, and P. Abbeel, "Domain randomization for transferring deep neural networks from simulation to the real world," in *2017 IEEE/RSJ international conference on intelligent robots and systems (IROS)*. IEEE, 2017, pp. 23–30.
- [38] O. M. Andrychowicz, B. Baker, M. Chociej, R. Jozefowicz, B. McGrew, J. Pachocki, A. Petron, M. Plappert, G. Powell, A. Ray *et al.*, "Learning dexterous in-hand manipulation," *The International Journal of Robotics Research*, vol. 39, no. 1, pp. 3–20, 2020.
- [39] I. Akkaya, M. Andrychowicz, M. Chociej, M. Litwin, B. McGrew, A. Petron, A. Paino, M. Plappert, G. Powell, R. Ribas *et al.*, "Solving rubik's cube with a robot hand," *arXiv preprint arXiv:1910.07113*, 2019.
- [40] E. Olson, "AprilTag: A robust and flexible visual fiducial system," in *Proceedings of the IEEE International Conference on Robotics and Automation (ICRA)*. IEEE, May 2011, pp. 3400–3407.